Soft Matter

View Online
Dynamic Article Links

Cite this: *Soft Matter*, 2011, **7**, 7797

www.rsc.org/softmatter

PAPER

Interfacial effects on droplet dynamics in Poiseuille flow†

Jonathan T. Schwalbe,*[a] Frederick R. Phelan, Jr.,[a] Petia M. Vlahovska[b] and Steven D. Hudson[a]

Received 27th January 2011, Accepted 10th March 2011
DOI: 10.1039/c1sm05144j

Many properties of emulsions arise from interfacial rheology, but a theoretical understanding of the effect of interfacial viscosities on droplet dynamics is lacking. Here we report such a theory, relating to isolated spherical drops in a Poiseuille flow. Stokes flow is assumed in the bulk phases, and a jump in hydrodynamic stress at the interface is balanced by Marangoni and surface viscous forces according to the Boussinesq–Scriven constitutive law. Our model employs a linear equation of state for the surfactant. Our analysis predicts slip, cross-stream migration and droplet-circulation velocities. These results and the corresponding interfacial parameters are separable: *e.g.*, cross-stream migration occurs only if gradients in surfactant concentration are present; slip velocity depends on viscosity contrast and dilatational properties, but not on shear Boussinesq number. This separability allows a new and advantageous means to measure surface viscous and elastic forces directly from the drop interface.

1. Introduction

Droplet dynamics in flow reflects a number of properties of the drop interface, and influences emulsion rheology and stability.[1] For some time now, it has been understood that droplets placed in a pressure-driven flow tend to be transported at a velocity less than that of the undisturbed flow. For example, a clean spherical viscous droplet lags behind the flow with a slip velocity given by (2) and undergoes no lateral migration.[2] In addition, depending on the viscosity contrast, deformable particles migrate either towards the flow centerline or away if initially placed off-center.[3–5] Recently, it was found that the presence of insoluble surfactant would induce a cross-stream migration in a spherical droplet.[6] In this case, the symmetry present in the spherical shape limit of a clean drop (prohibiting the lateral migration of the droplet[7]) is broken, and the spherical surfactant-covered droplet migrates toward the centerline of the flow.

Analysis of drop dynamics within the limit of Stokes flow and micron-sized droplets are not limited to theoretical studies. For example, migration of a droplet has been observed experimentally.[8,9] Additionally, experiments using a microfluidic interfacial tensiometer have been developed to probe interfacial dynamics and mass transfer processes for a micron-sized droplet in a confined rectangular channel.[10] Previous studies have yielded measurements of dynamic multi-component interfacial tension,[11,12] and insights into other processes such as tip streaming.[13,14]

Droplet dynamics in flow fields represents a long-standing problem, both theoretically and experimentally. However, investigation into the effects of surface viscous forces has been limited. In this work we generalize the results of Hanna and Vlahovska[6] to include the effects of surface viscous forces. Their results are for a drop which remains spherical by assuming that the capillary number is small; we adopt this assumption here as well. This aids isolation of the effects of the surfactant on the interface.

In order to avoid confusion when discussing interfaces free of surfactant, when no surface viscosity is present the interface is said to be *clean*. If surface viscosities are non-negligible (arising from some surface agent whose total concentration remains constant), the interface is referred to as being *viscous*. Interfacial viscosity and elasticity correlates to and retards the rate of droplet coalescence in emulsions.[15,16] Here we determine their effects on the dynamics of a spherical drop. We suggest that measurement of these quantities yields a new route to characterize interfacial viscosities, and therefore a new way to evaluate emulsion properties.

2. Problem formulation

In this study, we will consider a neutrally buoyant drop of radius a. The viscosity of the droplet is $\lambda\eta$ while the embedding ambient fluid has a viscosity of η. The drop interface is considered Newtonian, with surface shear viscosity μ^s and dilational viscosity κ^s The drop is placed in unbounded plane Poiseuille flow, $\mathbf{v}^\infty = (U' - \alpha y'^2)\hat{\mathbf{x}}$, where U' is the speed of the flow at the centerline, and α is proportional to the curvature of the flow profile. This flow is chosen because it excites both dilatational and shear deformations of the droplet, in similar magnitudes. We will consider initial drop locations both on and off the centerline

[a]*Complex Fluids Group, Polymers Division, National Institute of Standards and Technology, Gaithersburg, USA. E-mail: schwalbe@nist.gov; Fax: +1 301-975-4924; Tel: +1 301-975-6781*
[b]*Division of Engineering, Brown University, Rhode Island, USA*
† Official contribution of the National Institute of Standards and Technology; not subject to copyright in the United States.

of the flow. It therefore is convenient to express the applied velocity in a coordinate system centered on, and translating with the droplet. In dimensional units, the velocity profile is

$$\mathbf{v}^{\infty} = (-\dot{\gamma}y - \alpha y^2)\hat{\mathbf{x}} - \mathbf{U}'_{\mathrm{mig}} \tag{1}$$

where the local shear rate experienced by the drop is $\dot{\gamma} = 2\alpha y$, and y is the position of the droplet off the centerline of the flow. The migration velocity $\mathbf{U}'_{\mathrm{mig}}$ is the difference between the drop's velocity and the velocity of the undisturbed flow. In the absence of surface viscous forces,[2]

$$\mathbf{U}'_{\mathrm{mig}} = -\frac{\lambda}{3\lambda + 2}\alpha a^2 \hat{\mathbf{x}}. \tag{2}$$

We consider that the drop may be covered with an insoluble, non-diffusive, surfactant whose equilibrium concentration on the interface is given by Γ_{eq}. The corresponding tension in the membrane is σ_{eq}. When the interfacial surfactant concentration is uniform, the interface is *viscous*; Marangoni effects arise when the concentration has local variations.

In the absence of an imposed flow, the equilibrium shape of the droplet is spherical due to surface tension effects. If creeping flow conditions are assumed in the bulk phases, this shape can be maintained in the presence of flow if the capillary number, $\mathrm{Ca} = \eta U_c/\sigma_{\mathrm{eq}}$, remains small. Here U_c is the characteristic velocity, $U_c = \alpha a^2$. The strength of surface viscous forces relative to the bulk viscous forces acting on the interface are characterized by the dimensionless shear and dilational Boussinesq numbers,

$$\mathrm{Bo}^{\mathrm{s}} = \frac{\mu^{\mathrm{s}}}{\eta a}, \mathrm{Bo}^{\mathrm{d}} = \frac{\kappa^{\mathrm{s}}}{\eta a}. \tag{3}$$

Gradients in the surface tension may arise due to non-uniformities in the surfactant distribution stemming from convection of surfactant on the interface. The ratio of viscous stresses to these surface tension gradients defines the Marangoni number, $\mathrm{Ma}^{-1} = \eta U_c/[-\Gamma_{\mathrm{eq}}(\partial\sigma/\partial\Gamma)]$. The surface tension dependence on the local surfactant concentration is nonlinear for arbitrary concentrations.[17,18] Here, however, we assume a linear equation of state (for small deviations on local interfacial concentration Γ from its equilibrium value Γ_{eq})

$$\sigma(\Gamma) = \mathrm{Ma}(1 - \Gamma/\Gamma_{\mathrm{eq}}) + \sigma_{\mathrm{eq}}. \tag{4}$$

In general, it is possible that surface viscosities depend on the nonunifomities in Γ, but in the absence of any such model, we ignore this possibility, implying that Bo^{d} and Bo^{s} are functions of Γ_{eq} only. Henceforth, all variables are rescaled with a, η, σ_{eq}, Γ_{eq} as characteristic quantities.

2.1 Governing equations

The flow in the bulk phases is described using the Stokes equations, where the velocity $\mathbf{v}$ and pressure p satisfy

$$\nabla p = \hat{\eta}\nabla^2\mathbf{v}, \quad \nabla\cdot\mathbf{v} = 0, \tag{5}$$

with $\hat{\eta} = 1$ in the suspending fluid and $\hat{\eta} = \lambda$ in the droplet. The velocity field is continuous across the interface. Far from the droplet, the velocity tends to the unperturbed imposed flow. At the interface, the jump in the viscous hydrodynamic stresses is balanced by membrane surface forces,

$$\|\mathbf{T}^{\mathrm{hd}}\|\cdot\hat{\mathbf{n}} = -2H\sigma\hat{\mathbf{n}} + \nabla_{\mathrm{s}}\sigma - \nabla_{\mathrm{s}}\cdot\tau^{\mathrm{s}} \tag{6}$$

where ∇_{s} is the surface gradient operator, τ^{s} is the surface stress tensor, H is the mean curvature of the interface, $\hat{\mathbf{n}}$ is the outward point unit normal vector (for a sphere $\hat{\mathbf{n}} = \hat{\mathbf{r}}$), and $\|\ldots\|$ denotes a jump in the quantity enclosed from the inside to the outside. Here $\mathbf{T}^{\mathrm{hd}} = -p\mathbf{I} + \hat{\eta}[\nabla\mathbf{v} + (\nabla\mathbf{v})^{\dagger}]$ is the bulk hydrodynamic stress tensor, $\mathbf{I}$ is the unit tensor, and $\dagger$ denotes the transpose. For a spherical droplet, the dimensionless mean curvature is 1. The third term on the right-hand side of (6) is the force exerted on the interface from surface viscous effects. Adopting the Boussinesq–Scriven constitutive law for Newtonian interfaces gives[19]

$$\nabla_{\mathrm{s}}\cdot\tau^{\mathrm{s}} = 2\mathrm{Bo}^{\mathrm{s}}\mathbf{D}_{\mathrm{s}} + (\mathrm{Bo}^{\mathrm{d}} - \mathrm{Bo}^{\mathrm{s}})(\mathbf{I}_{\mathrm{s}}:\mathbf{D}_{\mathrm{s}})\mathbf{I}_{\mathrm{s}}. \tag{7}$$

where

$$\mathbf{D}_{\mathrm{s}} = \frac{1}{2}\left[\nabla_{\mathrm{s}}\mathbf{v}\cdot\mathbf{I}_{\mathrm{s}} + \mathbf{I}_{\mathrm{s}}\cdot(\nabla_{\mathrm{s}}\mathbf{v})^{\dagger}\right] \tag{8}$$

is the surface rate of deformation tensor, and $\mathbf{I}_{\mathrm{s}} = \mathbf{I} - \hat{\mathbf{n}}\hat{\mathbf{n}}$. Inserting (8) into (7) gives[19]

$$\begin{aligned}\nabla_{\mathrm{s}}\cdot\tau^{\mathrm{s}} &= (\mathrm{Bo}^{\mathrm{d}} + \mathrm{Bo}^{\mathrm{s}})\nabla_{\mathrm{s}}\nabla_{\mathrm{s}}\cdot\mathbf{v}\\ &+[2\mathrm{Bo}^{\mathrm{s}}\mathbf{b} : \nabla\mathbf{v} + (\mathrm{Bo}^{\mathrm{d}} + \mathrm{Bo}^{\mathrm{s}})2H\nabla_{\mathrm{s}}\cdot\mathbf{v}]\\ &+\mathrm{Bo}^{\mathrm{s}}[-\nabla_{\mathrm{s}}\times\nabla_{\mathrm{s}}\times\mathbf{v}_{\mathrm{s}} + K\mathbf{v}_{\mathrm{s}} + 2H(\nabla_{\mathrm{s}}\mathbf{v})\cdot\hat{\mathbf{n}} -\\ &2(\mathbf{b} - 2H\mathbf{I}_{\mathrm{s}})\cdot\nabla_{\mathrm{s}}(\mathbf{v}\cdot\hat{\mathbf{n}})]\end{aligned} \tag{9}$$

where $\mathbf{b} = -\nabla_{\mathrm{s}}\hat{\mathbf{n}}$, $\mathbf{v}_{\mathrm{s}} = \mathbf{I}_{\mathrm{s}}\cdot\mathbf{v}$, and K is the Gaussian curvature.

For a viscous interface with a constant tension $\sigma = \sigma_{\mathrm{eq}}$, (6) in conjunction with the conditions on the velocity field is sufficient to solve for the flow past the spherical droplet. On the other hand, if an insoluble surfactant is present and gradients in its interfacial concentration develop, (4) modifies (6),

$$\|\mathbf{T}^{\mathrm{hd}}\|\cdot\hat{\mathbf{n}} = 2\mathrm{Ma}(\Gamma - 1)\hat{\mathbf{n}} - \mathrm{Ma}\nabla_{\mathrm{s}}\Gamma - \nabla_{\mathrm{s}}\cdot\tau^{\mathrm{s}}. \tag{10}$$

In this situation, in order to close the problem, a conservation equation for the surfactant concentration is employed as an evolution equation for Γ,

$$\frac{\partial\Gamma}{\partial t} + \nabla_{\mathrm{s}}\cdot(\mathbf{v}_{\mathrm{s}}\Gamma) + \Gamma(\mathbf{v}\cdot\hat{\mathbf{n}})(\nabla\cdot\hat{\mathbf{n}}) = 0, \tag{11}$$

where any diffusion flux has been neglected. On a sphere, $\nabla\cdot\hat{\mathbf{n}} = 2$. Lastly, $\mathbf{v}_{\mathrm{s}}$ is the tangential surface velocity.

3. Solution for a spherical droplet

In the limit of a spherical droplet, exact expressions for the velocity field can be obtained as a function of λ, Bo^{s}, Bo^{d}, and, if present, the concentration of surfactant. From the linearity of the Stokes equations, the perturbation of the flow field about the surfactant-covered droplet can be decomposed into two parts: flow about a viscous drop, and flow induced from Marangoni stresses.[1] Therefore $\mathbf{U}_{\mathrm{mig}}$ will be decomposed as

$$\mathbf{U}_{\mathrm{mig}} = \mathbf{U}^0_{\mathrm{mig}} + \mathbf{U}^{\mathrm{s}}_{\mathrm{mig}}. \tag{12}$$

Henceforth, excluding previously defined terms, a superscript 's' will indicate terms arising from surfactant concentration gradient effects, and a superscript 0 will indicate a viscous interface. Owing to the spherical nature of the droplet, the spherical coordinate system, (r, θ, ϕ), is adopted and all fields are expanded in the basis of spherical harmonics (see Appendix A). Using spherical harmonics, the fundamental set of velocity fields is given by

$$\mathbf{v}_{\text{out}} = c^{\infty}_{jmq}[\mathbf{u}^{+}_{jmq}(\mathbf{r}) - \mathbf{u}^{-}_{jmq}(\mathbf{r})] + c_{jmq}\mathbf{u}^{-}_{jmq}(\mathbf{r})$$

$$\mathbf{v}_{\text{in}} = c_{jmq}\mathbf{u}^{+}_{jmq}(\mathbf{r}) \tag{13}$$

where summation over repeated indices is implied. Details of the basis functions, $\mathbf{u}^{\pm}_{jmq}(\mathbf{r})$, can be found in Appendix D.[1,20] Note that this velocity field is naturally continuous across the interface. The coefficients which define the far field velocity, $c_{jmq}{}^{\infty}$ can be found in Appendix C. Similar to (12), the coefficients c_{jmq} are decomposed as $c_{jmq} = c^{0}_{jmq} + c^{s}_{jmq}$. Moreover, in the limit of a spherical droplet, (9) simplifies by recognizing $K = 1$, and $\mathbf{b} = -\mathbf{I}_s$. Therefore, on a sphere, (9) reduces to

$$\begin{aligned}\nabla_s\cdot\tau^s &= (\text{Bo}^d + \text{Bo}^s)\nabla_s\nabla_s\cdot\mathbf{v} - 2\text{Bo}^s(\nabla_s\cdot\mathbf{v})\hat{\mathbf{r}} \\ &+ \text{Bo}^s[\nabla_s\times\nabla_s\times\mathbf{v}_s + 3\mathbf{v}_s - 2\nabla_s(\mathbf{v}\cdot\hat{\mathbf{r}})].\end{aligned} \tag{14}$$

3.1 Viscous interface solution

Neglecting the effects of surfactant concentration gradients, the coefficients c_{jmq} are determined from the stress balance given by (6). The condition that the drop remains spherical places an extra constraint on the system, which overdetermines it if both the normal and tangential components of (6) are employed.[6] In order to maintain sphericity, $c_{jm2} = 0$ for $j > 1$ leaving c_{jm0} and c_{jm1} to be determined from the tangential components of (6). For $j = 1$, all three components of (6) are used. Additionally, in order to maintain sphericity, the jump in hydrostatic pressure across the interface is balanced by a large tension ($\text{Ca} \ll 1$) and therefore the effects of σ_{eq} are not felt here.

Expressed in component form, (6), in conjunction with the spherical harmonic expansion of (9) becomes,

$$\begin{aligned}\tau^{\text{out}}_{jm0} - \tau^{\text{in}}_{jm0} &= -2\text{Bo}^d\sqrt{j(j+1)}c^0_{jm2} \\ &+\left[\text{Bo}^s(j+2)(j-1) + \text{Bo}^d j(j+1)\right]c^0_{jm0}\end{aligned} \tag{15}$$

$$\tau^{\text{out}}_{jm1} - \tau^{\text{in}}_{jm1} = \text{Bo}^s(j+2)(j-1)c^0_{jm1} \tag{16}$$

$$\tau^{\text{out}}_{jm2} - \tau^{\text{in}}_{jm2} = 2\text{Bo}^d\left[2c^0_{jm2} - \sqrt{j(j+1)}c^0_{jm0}\right] \tag{17}$$

Solving the above system for the coefficients c_{jmq} yields, for $j = 1$,

$$\begin{aligned}c^0_{1m0} &= \frac{1}{3\beta}\left[\sqrt{2}\hat{\beta}c^{\infty}_{1m2} + (9 + 4\text{Bo}^d + 6\lambda)c^{\infty}_{1m0}\right] \\ c^0_{1m1} &= c^{\infty}_{1m1} \\ c^0_{1m2} &= \frac{1}{3\beta}\left[\sqrt{2}\hat{\beta}c^{\infty}_{1m0} + (12 + 2\text{Bo}^d + 3\lambda)c^{\infty}_{1m2}\right]\end{aligned} \tag{18}$$

where $\beta = 2 + 2\text{Bo}^d + 3\lambda$ and $\hat{\beta} = 2\text{Bo}^d - 3 + 3\lambda$. When $j > 1$ we have

$$\begin{aligned}c^0_{jm0} &= \frac{2j+1}{\sqrt{j(j+1)}}\left(\frac{2\sqrt{j(j+1)}c^{\infty}_{jm0} - 3c^{\infty}_{jm2}}{1 + \lambda - 2\text{Bo}^s + j\delta}\right) \\ c^0_{jm1} &= \frac{1}{\delta}(2j+1)c^{\infty}_{jm1} \\ c^0_{jm2} &= 0\end{aligned} \tag{19}$$

where $\delta = 2 + 2\lambda + (1 + j)(\text{Bo}^s + \text{Bo}^d)$. Note how when $j = 1$, Bo^s does not enter c_{1mq}, and when $\text{Bo}^d = 0$, and $\text{Bo}^s = 0$, the solution was previously identified by Hanna and Vlahovska.[6] Obtaining an expression for the migration velocity similar to (2) requires determining the difference between the undisturbed imposed flow and the volume averaged velocity of the drop,

$$\mathbf{U}_{\text{mig}} = -\mathbf{v}^{\infty}(0) + \frac{3}{4\pi}\int_{\text{drop}}\mathbf{v}(\mathbf{r})\,d\mathbf{r}. \tag{20}$$

The only nonzero contribution to this integral are the $\mathbf{u}^{+}_{1m2}$ modes, yielding

$$\mathbf{U}_{\text{mig}} = \sqrt{\frac{3}{8\pi}}\left[-(c_{112} - c_{1-12})\hat{\mathbf{x}} - \text{i}(c_{112} + c_{1-12})\hat{\mathbf{y}} + \sqrt{2}c_{102}\hat{\mathbf{z}}\right] \tag{21}$$

This shows that the migration velocity of a spherical droplet is only given by the $j = 1$ modes. In the absence of surfactant, these modes are not coupled to any other of higher order, and the solution can be given in closed form.

3.2 Marangoni effects

The presence of interfacial viscous forces does not change the functional form of the c^{s}_{jmq} previously reported (6), and are reproduced in Appendix F for completeness. Motivated by the expansion of the velocity fields (13) in spherical harmonics, the local surfactant concentration, $\Gamma(\theta,\phi,t)$, will be expanded in scalar harmonics as

$$\Gamma(\theta,\phi,t) = 1 + \sum_{j=1}^{\infty}\sum_{m=-j}^{j} g_{jm}(t)\,Y_{jm}(\theta,\phi). \tag{22}$$

Use of (11) along with (22) and (54) yields the evolution equation for the coefficients g_{jm}

$$\begin{aligned}\frac{\partial g_{jm}}{\partial t} &= C_{jm} + \left[\Omega_{jmj_2m_2} + \Lambda_{jmj_2m_2}\right]g_{j_2m_2} \\ &+\text{Ma}\left[W(j)g_{jm} + \Psi_{jmj_1m_1j_2m_2}g_{j_2m_2}g_{j_1m_1}\right]\end{aligned} \tag{23}$$

It was noted previously that, for either a clean ($\Gamma = 0$) or viscous ($\Gamma = 1$) interface, all harmonic modes are decoupled. The nonlinear nature of (23) shows that the presence of surfactant concentration gradients couples the modes together. Specific details concerning the terms in (23) are given in Appendix F.

Once the amplitudes g_{jm} are obtained, the decomposition of c_{jmq} gives

$$\mathbf{U}^{s}_{\text{mig}} = \frac{\text{Ma}}{\sqrt{6\pi}(3\lambda+2)}\left[-(g_{11} - g_{1-1})\hat{\mathbf{x}} - \text{i}(g_{11} + g_{1-1})\hat{\mathbf{y}} + \sqrt{2}g_{10}\hat{\mathbf{z}}\right] \tag{24}$$

as a migration velocity induced by gradients in surfactant concentration.[6]

4. Results and discussion

In this section, first the results concerning a viscous interface are shown, which include analytical expressions for a new slip velocity and drop fluid circulation patterns observable in laboratory experiments. Following that discussion, surfactant gradient effects are introduced, the asymptotic limit of an incompressible interface is explored, and the lateral migration velocity is calculated as a function of Bo^s and Bo^d. Lastly, numerical solutions for arbitrary surfactant concentration gradients are discussed.

4.1 Viscous interface

To begin, we derive here the slip velocity of a drop with surface viscosity and without surfactant concentration gradients. Inserting the appropriate terms from (18), (19) and (47) into (21) yields

$$\mathbf{U}_{\mathrm{mig}} = -\frac{2\mathrm{Bo}^{\mathrm{d}} + 3\lambda}{3(2 + 2\mathrm{Bo}^{\mathrm{d}} + 3\lambda)}\hat{\mathbf{x}}. \tag{25}$$

In the limit of either high drop viscosity, or large dilational viscosity, the rigid sphere slip migration is recovered, namely $\mathbf{U}_{\mathrm{mig}} = -{}^1/_3\,\hat{\mathbf{x}}$.[7] Moreover, it should be noted that the above slip velocity is independent of the shear surface viscosity, Bo^s, a result of the fact that Bo^s does not appear in (18). Therefore, if Bo^s is small and Bo^d is large, there is fluid circulation in the drop, yet it lags behind the flow as for a rigid sphere. As a final comment, when $Bo^d = 0$, (25) reduces to (2). The absence of Bo^s dependence in the slip velocity is in agreement with Felderhof,[21] who found that the velocity and pressure fields produced by a droplet's response to a uniform flow are independent of the interfacial shear viscosity.

Circulation patterns are readily measured experimentally.[10] Previous theory[22] considered the circulation patterns within and on a droplet in microchannels. The velocity field at various locations on the droplet was determined; however, these results do not account for the interfacial viscous forces. Several points are indicated on the droplet in Fig. 1 which will be of interest to us here. The velocity field given by (13) is converted to the Cartesian coordinate system to highlight various velocity components on and within the drop. In order to illustrate only the circulation patterns, the slip velocity (25) has been removed from the velocity field. Additionally, the drop is assumed to be on the centerline of the flow ($y_0 = 0$). The x-component of the velocities at points A and B are

$$v_x(\mathrm{A}) = \frac{5}{3(4 + 4\mathrm{Bo}^{\mathrm{s}} + \lambda)} - \frac{1}{2 + 2\mathrm{Bo}^{\mathrm{d}} + 3\lambda} + \frac{7}{12\nu} \tag{26}$$

and

$$v_x(\mathrm{B}) = -\frac{5}{3(4 + 4\mathrm{Bo}^{\mathrm{s}} + \lambda)} - \frac{1}{2 + 2\mathrm{Bo}^{\mathrm{d}} + 3\lambda} - \frac{7}{3\nu} \tag{27}$$

where $\nu = 7(1 + \lambda) + 12\mathrm{Bo}^{\mathrm{d}} + 10\mathrm{Bo}^{\mathrm{s}}$. These velocity components are dependent on the values of both Bo^d and Bo^s. Fluid at the center of the droplet, denoted by point C, has an x velocity component given by

$$v_x(\mathrm{C}) = \frac{1}{2 + 2\mathrm{Bo}^{\mathrm{d}} + 3\lambda} \tag{28}$$

which clearly has no dependence on Bo^s. In the limit of large Bo^d this becomes $v_x(\mathrm{C}) = 0$. The other velocity components here are zero for all values of the parameters (at $y_0 = 0$). In (25) and (28) we have isolated velocities that depend only on λ and Bo^d; a velocity independent of Bo^s would be ideal as well. The following combination of points A, B, and C yield an x-velocity which depends only on λ and Bo^s,

$$\frac{4}{5}v_x(\mathrm{A}) + \frac{1}{5}v_x(\mathrm{B}) + v_x(\mathrm{C}) = \frac{1}{4 + 4\mathrm{Bo}^{\mathrm{s}} + \lambda}. \tag{29}$$

The combination $\frac{4}{5}v_x(\mathrm{A}) + \frac{1}{5}v_x(\mathrm{B})$ can be obtained from the interfacial velocity measured 26° from the azimuthal axis from A towards B.

Fig. 2 shows streamlines within the droplet in the x–y coordinate plane. The figure contains three parts. In Fig. 2a, the shear and dilational Boussinesq numbers are zero. Effects of Bo^d become apparent in Fig. 2b, where $Bo^d = 10$ while $Bo^s = 0$. The magnitude of the fluid velocity near the center of the drop has greatly decreased. Lastly, the influence of Bo^s is isolated in Fig. 2c in the case of $Bo^s = 10$ and $Bo^d = 0$. Streamline profiles with other combinations of Bo^d and Bo^s are readily calculated; in general, these are not qualitatively different from what is shown in Fig. 2.

The position of the stagnation points located along the y axis (y_s) are given by solutions of the following 4th-order polynomial equation for y_s

$$0 = \frac{5y_s^2}{4 + 4\mathrm{Bo}^{\mathrm{s}} + \lambda} + \frac{3(2y_s^2 - 1)}{2 + 2\mathrm{Bo}^{\mathrm{d}} + 3\lambda} + \frac{7}{\nu}y_s^2(3y_s^2 - 2). \tag{30}$$

It should be noted that although four solutions to (30) exist, only one of them satisfies the criteria that it be both real and less than one. Although analytical solutions to (30) exist, a more illustrative discussion of these solutions is obtained by examining the limit of large Boussinesq number. In the limit of $\mathrm{Bo}^{\mathrm{d}} \to \infty$, only the first term in (30) survives, therefore $y_s = 0$. On the other hand, in the limit of $\mathrm{Bo}^{\mathrm{s}} \to \infty$, the second term in (30) survives, giving the condition $y_s = \pm 1/\sqrt{2} \approx 0.707$.

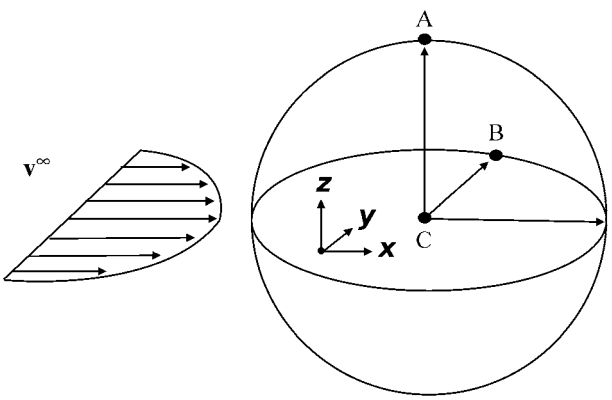

Fig. 1 Schematic of the droplet and velocity profile. Points of interest are marked on and in the drop.

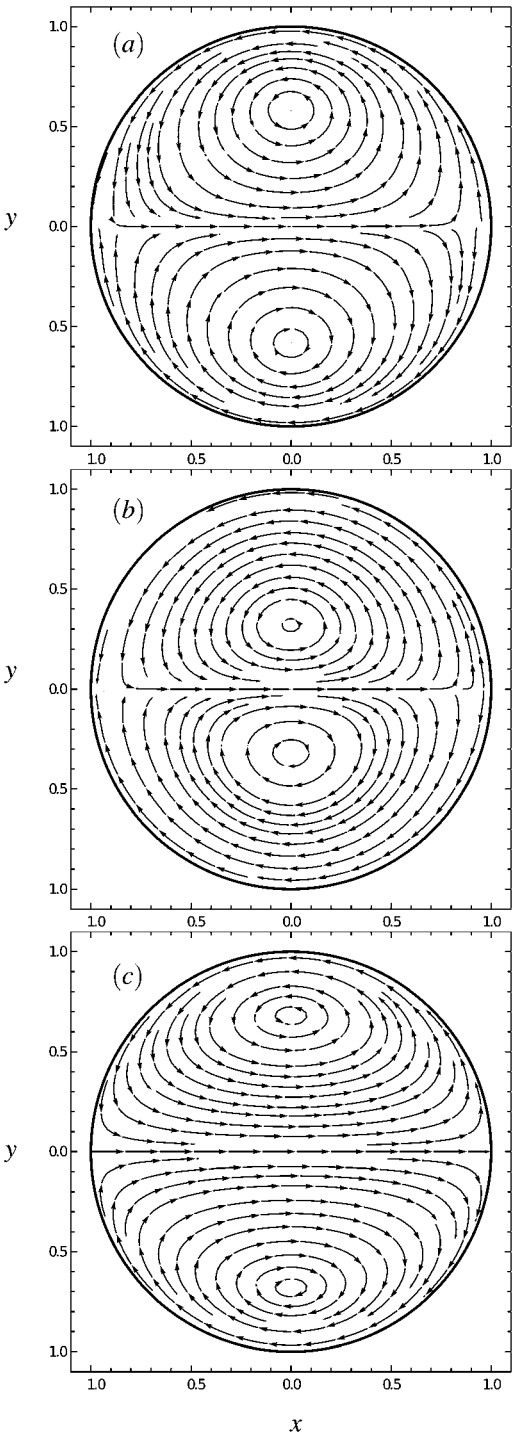

Fig. 2 Fluid velocity field within the droplet in the x–y plane. $\lambda = 1$ for all plots. In (*a*), $\mathrm{Bo^d} = \mathrm{Bo^s} = 0$, (*b*), $\mathrm{Bo^d} = 10$, $\mathrm{Bo^s} = 0$, and in (*c*), $\mathrm{Bo^d} = 0$, and $\mathrm{Bo^s} = 10$.

4.2 Marangoni effects

In this section the effects of interfacial surfactant concentration gradients are explored. Both analytical results within asymptotic limits and numerical results are presented.

To begin, (23) is solved in the quasi-steady state, and it is assumed that surfactant redistribution to its equilibrium value dominates convection effects. Within this limit, Ma^{-1} is the relevant small parameter in the problem. Both the migration velocity $\mathbf{U}_{\mathrm{mig}}$ and g_{jm} therefore admit regular perturbation expansions,

$$\mathbf{U}_{\mathrm{mig}} = \mathbf{U}^{(0)}_{\mathrm{mig}} + \mathrm{Ma}^{-1}\mathbf{U}^{(1)}_{\mathrm{mig}} + \ldots,$$
$$g_{jm} = g^{(0)}_{jm} + \mathrm{Ma}^{-1} g^{(1)}_{jm} + \ldots. \tag{31}$$

The leading-order result is that shear and dilational surface viscosities do not remobilize the interface in this limit of an incompressible surfactant; the slip velocity is that of a rigid sphere, $\mathbf{U}^{(0)}_{\mathrm{mig}} = -{}^1\!/_3\,\hat{\mathbf{x}}$. See Appendix G for expressions for $g^{(0)}_{jm}$. This is the same limit obtained for large $\mathrm{Bo^d}$ in (25), which is another way an incompressible interface can be obtained within the context of this problem. Thus, as regards steady-state interfacial dilatation, both high elasticity or dilational viscosity achieve the same limit.

At the next order in perturbation the relevant terms in (23) are

$$0 = \left[\Omega_{jmj_2m_2} + \Lambda_{jmj_2m_2}\right] g^{(0)}_{j_2m_2} + W(j) g^{(1)}_{jm} + \Psi_{jmj_1m_1j_2m_2} g^{(0)}_{j_1m_1} g^{(0)}_{j_2m_2} \tag{32}$$

Solving the above for $g^{(1)}_{\pm 1}$ and inserting it into (24) and using (31) we find that a cross-stream (lateral) migration enters the system

$$\mathbf{U}^{(1)}_{\mathrm{mig}} = y_0 \Big\{ (2\lambda+3)\left[48(\mathrm{Bo^s})^2 + 36\mathrm{Bo^s}(3+2\lambda) + 5(1+\lambda)(17+3\lambda)\right] + 2\mathrm{Bo^d}\left[97 + 36\mathrm{Bo^s}(2+3\lambda) + \lambda(151+27\lambda)\right]\hat{\delta}^{-1}\hat{y}, \tag{33}$$

where

$$\hat{\delta} = 9(4 + 4\mathrm{Bo^s} + \lambda)(2 + 2\mathrm{Bo^d} + 3\lambda)(5 + 6\mathrm{Bo^d} + 4\mathrm{Bo^s} + 5\lambda). \tag{34}$$

Surfactant gradients induce a cross-stream migration of the drop in the flow. This effect is not seen in the incompressible limit of a clean (or viscous interface) spherical drop. This migration velocity depends linearly on y_0, and is directed towards the flow centerline for all values of λ, $\mathrm{Bo^d}$, and $\mathrm{Bo^s}$.

When $\mathrm{Bo^d} = \mathrm{Bo^s} = 0$, $\mathbf{U}^{(1)}_{\mathrm{mig}}\cdot\hat{\mathbf{y}}$ decreases monotonically with increasing λ until a rigid-sphere limit is reached. On the other hand, if $\mathrm{Bo^d} > 0$, $\mathbf{U}^{(1)}_{\mathrm{mig}}\cdot\hat{\mathbf{y}}$ approaches the rigid-sphere limit either monotonically ($\mathrm{Bo^d} > \mathrm{Bo^d_c}$) or non-monotonically ($\mathrm{Bo^d} > \mathrm{Bo^d_c}$). Here $\mathrm{Bo^d_c}$ is the value of $\mathrm{Bo^d}$ below which (33) has an extremum on the positive λ line, and above which it does not. This behavior is seen in Fig. 3a. If, on the other hand, $\mathrm{Bo^s}$ were varied while keeping $\mathrm{Bo^d} = 0$, non-monotonic behavior is seen in $\mathbf{U}^{(1)}_{\mathrm{mig}}$ (see Fig. 3b). In the limit of large $\mathrm{Bo^s}$, $\mathbf{U}^{(1)}_{\mathrm{mig}} = {}^1\!/_3\,\hat{\mathbf{y}}$ for all values of λ. It should be noted that in the limit of large λ, the addition of the surface viscous forces does not modify the conclusions reached in ref. 6. In the presence of both shear and dilatational forces, dilatation dominates, and thus the addition of even large values $\mathrm{Bo^s}$ (*e.g.* 10^3) results in only a minor change to the curves in Fig. 3a.

Results for an arbitrary distribution of surfactant on the surface can be obtained by solving (23) numerically. In this case, all modes are coupled and the (23) represents an infinite sum. For numerical convenience, the series is truncated at the $j = 6$ harmonic mode. The trajectory of the droplet in the channel ($y_s(t)$) is found by numerically solving

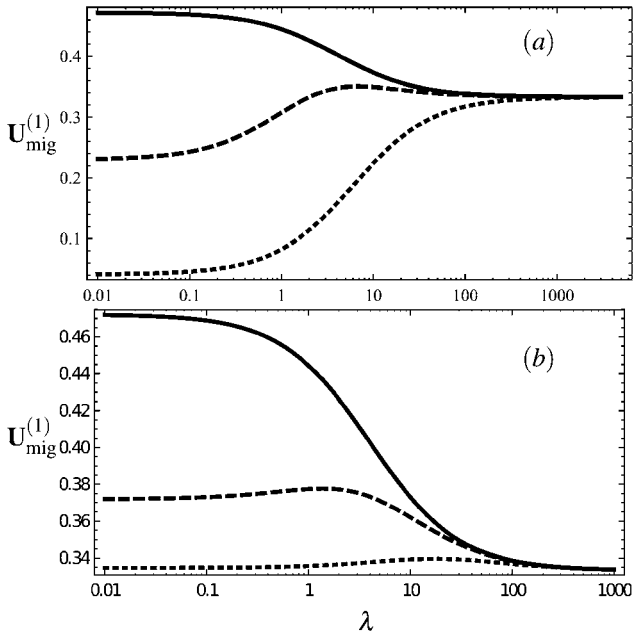

Fig. 3 Marangoni-induced lateral migration velocity as a function of λ. In (*a*) the solid, dashed and dotted curves are for $Bo^d = 0$, 1, 10, respectively, while $Bo^s = 0$. In (*b*) the solid, dashed and dotted curves are for $Bo^s = 0$, 1, 10, respectively, while $Bo^d = 0$.

$$\frac{dy_s}{dt} = \mathbf{U}_{mig}[y_s, \Gamma(y_s)] \cdot \hat{\mathbf{y}}. \tag{35}$$

Previous works on capsules[23,24] found that the motion of an object in unbounded parabolic flow is directed towards the centerline of the flow. This observation is consistent with the results of Fig. 4, where the trajectory, y_s, is shown for a spherical surfactant-covered droplet. Increasing either Bo^d or Bo^s will increase the time needed for the drop to reach the equilibrium centerline of the flow field. However, dilatational surface viscosity severely delays cross-stream migration of the droplet, while the effects of shear surface viscosity effects are not as strong. Surfactant concentration profiles are qualitatively similar to those of Fig. 2 in Hanna and Vlahovska,[6] and are essentially combinations of $j = 3$ and $j = 2$ harmonic modes.

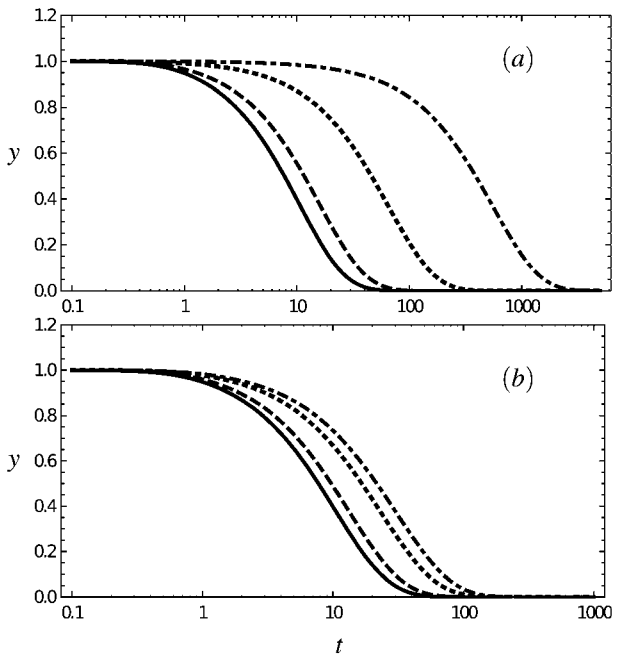

Fig. 4 Trajectories of the droplet in Poiseuille flow. In (*a*) the solid, dashed, dotted, and dot-dashed curves are for $Bo^d = 0$, 1, 10, 100, respectively, while $Bo^s = 0$, $Ma = 10$, and $\lambda = 1$. In (*b*) the solid, dashed, dotted and dot-dashed curves are for $Bo^s = 0$, 1, 10, 100, respectively, while $Bo^d = 0$, $Ma = 10$, and $\lambda = 1$.

5. Conclusions

We have shown here that interfacial viscous forces can modify the dynamics of a spherical droplet in a plane unbounded Poiseuille flow. A modified slip velocity was found which depends only on the viscosity of the drop and surface dilatation. Additionally, several locations on and within the drop were found where components of the velocity field were either independent of Bo^d or Bo^s, or where a combination eliminated the dependence of one Boussinesq number. These points are ideal locations for experimental measurements to obtain information about surface viscosities.

When Marangoni effects (*i.e.* concentration gradients in surfactant) are considered, the limit of incompressibility reveals a slip coefficient identical to that of a clean droplet with high surface dilational viscosity. Concentration gradients still break the symmetry and induce a cross-stream migration. For arbitrary surfactant concentrations, drop trajectories were numerically found which highlight the effects of surface viscous forces.

Whether for viscous interfaces or those where surfactant concentration is explicit, we have considered the effect of an interfacial agent, *i.e.*, of some agent which forms on the interface and modifies its properties. The viscous interface was assumed to have constant properties if other transport mechanisms are sufficiently active to maintain a uniform concentration of interfacial agents. Motivated by the results obtained here, an investigation into deformable droplets in flow with viscous interfaces is warranted.

Appendix A – Spherical harmonics

The normalized scalar spherical harmonics are defined as

$$Y_{jm}(\theta, \phi) = \left[\frac{2j+1}{4\pi}\frac{(j-n!)}{(j+n)!}\right]^{\frac{1}{2}}(-1)^m P_j^m(\cos\theta)e^{im\phi}, \tag{36}$$

where $P_j^m(\cos\theta)$ are the associated Legendre polynomials. From the scalar harmonics, the vector spherical harmonics relevant to our study are defined as[1]

$$\begin{aligned} \mathbf{y}_{jm0} &= [j(j+1)]^{-1/2} r\nabla_\Omega Y_{jm}, \\ \mathbf{y}_{jm1} &= -i\hat{\mathbf{r}} \times \mathbf{y}_{jm0}, \\ \mathbf{y}_{jm2} &= \hat{\mathbf{r}} Y_{jm}, \end{aligned} \tag{37}$$

where ∇_Ω is the angular part of the gradient operator in spherical coordinates.

Appendix B – Coupling of scalar and vector harmonics

Within this study, the coupling between scalar and vector spherical harmonics is inevitable. In this section, formulas developed in ref. 25 and given in ref. 26 for this coupling are shown for completeness. The product of scalar harmonics is recoupled as

$$Y_{jm}Y_{j_1m_1} = 2\zeta(j,j_1,j_2,m,m_1,m_2,2)\,Y_{j_2m_2}. \tag{38}$$

Summation over repeated indices is implied. The coupling formula between scalar and vector harmonics is

$$\mathbf{y}_{jmq}Y_{j_1m_1} = \mathbf{C}_{qq2}(j,j_1,j_2) \times \zeta(j,j_1,j_2,m,m_1,m_2,2)\mathbf{y}_{j_2m_2q_2}. \tag{39}$$

The entries in the coupling matrix $\mathbf{C}_{qq2}$ are

$$\begin{aligned} C_{00} &= C_{11} = [j(j+1)j_2(j_2+1)]^{1/2}\chi(j,j_1,j_2),\\ C_{01} &= C_{10} = -[j(j+1)j_2(j_2+1)]^{1/2}\theta(j,j_1,j_2),\\ C_{22} &= 2. \end{aligned} \tag{40}$$

All other entries are zero. In the above,

$$\chi(j,j_1,j_2) = j(j+1) + j_2(j_2+1) - j_1(j_1+1) \tag{41}$$

and

$$\theta(j,j_1,j_2) = [(j+j_1-j_2)(1-j+j_1+j_2) \times (j-j_1+j_2)(1+j+j_1+j_2)]^{1/2} \tag{42}$$

The coupling between two vector harmonics produces a scalar harmonic in the following way

$$\mathbf{y}_{jmq}\mathbf{y}_{j_1m_1q_1} = \mathbf{C}_{qq_2}(j,j_1,j_2)(-1)^{\delta_{q_2\delta_{q_1}}} \times \zeta(j,j_1,j_2,m,m_1,m_2,2)\,Y_{j_2m_2}. \tag{43}$$

In (38), (39), and (43), ζ are the Clebsch–Gordon coefficients

$$\begin{aligned} &\zeta(j,j_1,j_2,m,m_1,m_2,2) =\\ &\frac{(-1)^{m_2}}{2}\left[\frac{(2j+1)(2j_1+1)(2j_2+1)}{4\pi}\right]^{1/2}\\ &\times\begin{pmatrix} j-\xi & j_1 & j_2\\ 0 & 0 & 0\end{pmatrix}\begin{pmatrix} j & j_1 & j_2\\ m & m_1 & -m_2\end{pmatrix} \end{aligned} \tag{44}$$

where $\xi = 0$ is $q + q_2$ is odd, and $\xi = 1$ if $q + q_2$ is either even or zero. Lastly,

$$\begin{pmatrix} j & j_1 & j_2\\ m & m_1 & m_2\end{pmatrix} \tag{45}$$

is the Wigner 3j symbol.[25] Properties of the 3j symbol can be found in ref. 26. For later convenience, let

$$\mathcal{G}^{q_1q_2}_{jmj_1m_1j_2m_2} = \mathbf{C}_{qq_2}(j,j_1,j_2)(-1)^{\delta_{q^2}\delta_{q1^2}} \times \zeta(j,j_1,j_2,m,m_1,m_2,2) \tag{46}$$

Appendix C – Coefficients of unbounded plane Poiseuille flow

For completeness, in this section, the coefficients, c_{jmq}, for plane Poiseuille flow are given. The full flow field is therefore given by $\mathbf{v}^{\infty} = c^{\infty}_{jmq}\mathbf{u}^{+}_{jmq}(\mathbf{r})$. These were taken from ref. 6 and are

$$\begin{aligned} c^{\infty}_{3\pm30} &= \mp\alpha\sqrt{\frac{4\pi}{105}}, c^{\infty}_{3\pm32} = \mp\alpha\sqrt{\frac{\pi}{35}}\\ c^{\infty}_{3\pm10} &= \mp\alpha\frac{2}{15}\sqrt{\frac{\pi}{7}}, c^{\infty}_{3\pm12} = \mp\alpha\frac{1}{5}\sqrt{\frac{\pi}{21}}\\ c^{\infty}_{2\pm20} &= \pm\mathrm{i}\dot{\gamma}\sqrt{\frac{\pi}{5}}, c^{\infty}_{2\pm22} = \pm\mathrm{i}\dot{\gamma}\sqrt{\frac{2\pi}{15}}\\ c^{\infty}_{2\pm11} &= \alpha\frac{1}{3}\sqrt{\frac{\pi}{5}}, c^{\infty}_{1\pm01} = \mathrm{i}\dot{\gamma}\sqrt{\frac{2\pi}{3}}\\ c^{\infty}_{1\pm10} &= \pm\left[\alpha\frac{4}{5} + \left(U^{x}_{\mathrm{mig}} \mp \mathrm{i}U^{y}_{\mathrm{mig}}\right)\right]\sqrt{\frac{\pi}{3}}\\ c^{\infty}_{1\pm12} &= \pm\left[\alpha\frac{1}{5} + \left(U^{x}_{\mathrm{mig}} \mp \mathrm{i}U^{y}_{\mathrm{mig}}\right)\right]\sqrt{\frac{2\pi}{3}}\\ c^{\infty}_{100} &= -2U^{z}_{\mathrm{mig}}\sqrt{\frac{2\pi}{3}}, c^{\infty}_{102} = -2U^{z}_{\mathrm{mig}}\sqrt{\frac{\pi}{3}} \end{aligned} \tag{47}$$

Appendix D – Fundamental set of velocity fields

Following the definitions given in Blawzdziewicz *et al.*,[1] we list the expressions for the functions $\mathbf{u}^{\pm}_{jmq}(r,\theta,\varphi)$. The velocity field outside the vesicle is described by

$$\begin{aligned} \mathbf{u}^{-}_{jm0} &= \frac{1}{2}r^{-j}(2-j+jr^{-2})\mathbf{y}_{jm0} +\\ &\frac{1}{2}r^{-j}[j(j+1)]^{1/2}(1-r^{-2})\mathbf{y}_{jm2}, \end{aligned} \tag{48a}$$

$$\mathbf{u}^{-}{}_{jm1} = r^{-j-1}\mathbf{y}_{jm1} \tag{48b}$$

$$\begin{aligned} \mathbf{u}^{-}_{jm2} &= \frac{1}{2}r^{-j}(2-j)\left(\frac{j}{1+j}\right)^{1/2}(1-r^{-2})\mathbf{y}_{jm0} +\\ &\frac{1}{2}r^{-j}(j+(2-j)r^{-2})\mathbf{y}_{jm2}. \end{aligned} \tag{48c}$$

The velocity field inside the vesicle is described by

$$\begin{aligned} \mathbf{u}^{+}_{jm0} &= \frac{1}{2}r^{j-1}(-(j+1)+(j+3)r^{2})\mathbf{y}_{jm0} -\\ &\frac{1}{2}r^{j-1}[j(j+1)]^{1/2}(1-r^{2})\mathbf{y}_{jm2}\ , \end{aligned} \tag{49a}$$

$$\mathbf{u}^{+}{}_{jm1} = r^{j}\mathbf{y}_{jm1} \tag{49b}$$

$$\begin{aligned} \mathbf{u}^{+}_{jm2} &= \frac{1}{2}r^{j-1}(3+j)\left(\frac{j+1}{j}\right)^{1/2}(1-r^{2})\mathbf{y}_{jm0} +\\ &\frac{1}{2}r^{j-1}(j+3-(j+1)r^{2})\mathbf{y}_{jm2}\ . \end{aligned} \tag{49c}$$

On a sphere with $r = 1$ these velocity fields reduce to the vector spherical harmonics defined by (37)

$$\mathbf{u}^{\pm}_{jmq} = \mathbf{y}_{jmq}. \tag{50}$$

Hence, $\mathbf{u}^{\pm}_{jm0}$ is tangential, and $\mathbf{u}^{\pm}_{jm2}$ is normal to a sphere. In addition, $\mathbf{u}^{\pm}_{jm0}$ defines an irrotational velocity field.

Appendix E – Hydrodynamic tractions

The hydrodynamic tractions associated with the velocity fields (13) can be represented in vector spherical harmonics, $\mathbf{T}^{\mathrm{hd}}\cdot\hat{\mathbf{n}} = \tau_{jmq}\mathbf{y}_{jmq}$,[27] where

$$\tau^{\text{out}}_{jmq} = c^{\infty}_{jmq'}\left(\Theta^{+}_{q'q} - \Theta^{-}_{q'q}\right) + c_{jmq'}\Theta^{-}_{q'q}$$
$$\tau^{\text{in}}_{jmq} = \lambda c_{jmq'}\Theta^{+}_{q'q} \tag{51}$$

where summation over q' is implied. The symmetric matrices $\Theta^{\pm}_{q'q}$ are

$$\Theta^{\pm}_{q'q} = \begin{pmatrix} 2j+1 & 0 & -3\sqrt{\dfrac{j+1}{j}} \\ 0 & j-1 & 0 \\ -3\sqrt{\dfrac{j+1}{j}} & 0 & 2j+1+\dfrac{3}{j} \end{pmatrix}, \tag{52}$$

$$\Theta^{-}_{q'q} = \begin{pmatrix} 2j-1 & 0 & -3\sqrt{\dfrac{j}{j+1}} \\ 0 & -j-1 & 0 \\ -3\sqrt{\dfrac{j+1}{j}} & -2j-1 & -\dfrac{3}{j+1} \end{pmatrix} \tag{53}$$

The reader should note that the indexing of the matrices begins with 0.

Appendix F – Surfactant-induced velocity field and evolution equations

The Marangoni terms present in (10) give rise to the following coefficients found in ref. 6:

$$c^{s}_{jm0} = -\frac{\delta_{1j}}{2\lambda+2}\frac{\sqrt{2}}{3}\text{Ma}\, g_{jm} - \frac{(1-\delta_{1j})}{1+\lambda}\text{Ma}\, g_{jm}$$
$$c^{s}_{jm1} = 0 \tag{54}$$
$$c^{s}_{jm2} = \frac{\delta_{1j}}{3\lambda+2}\frac{2}{3}\text{Ma}\, g_{jm}$$

where as before, δ_{ij} is the Kronecker delta.

The terms present in (23) are of two forms: clean drop and surfactant terms. The clean drop terms are

$$C_{jm} = \sqrt{j(j+1)}c^{0}_{jm0} - 2c^{s}_{jm2}$$
$$\Omega_{jmj_2m_2} = \sqrt{j(j+1)}\mathcal{G}^{01}_{jmj_1m_1j_2m_2}c^{0}_{j_1m_11} \tag{55}$$
$$\Lambda = \sqrt{j(j+1)}\mathcal{G}^{00}_{jmj_1m_1j_2m_2}c^{0}_{j_1m_10} - 2\mathcal{G}^{22}_{jmj_1m_1j_2m_2j-m}c^{0}_{j_1m_12}$$

The Ω term gives distortions in the surfactant-concentration-driven linear shear components of the flow, while C and Λ describe other effects. Making the definition $c^{s}_{jmq} = \bar{W}_{q}(j)\text{Mag}_{jm}$, the surfactant terms become

$$W(j) = \sqrt{j(j+1)}\,\overline{W}_0(j) - 2\overline{W}_2(j)$$
$$\Psi_{jmj_1m_1j_2m_2} = \sqrt{j(j+1)}\,\overline{W}_0(j_1)\mathcal{G}^{00}_{j_1m_1j_2m_2j-m} - 2\overline{W}_2(j_1)\mathcal{G}^{22}_{j_1m_1j_2m_2j-m} \tag{56}$$

Appendix G – Expressions for g_{jm}

In the limit of a nearly incompressible surfactant ($\text{Ma}^{-1} \ll 1$), the leading-order evolution equation for g_{jm} (23) admits the following solution for $j = 1$

$$g^{(0)}_{1m} = \frac{2+3\lambda}{2+2\text{Bo}^{\text{d}}+3\lambda}\Big[\sqrt{2}(2\text{Bo}^{\text{d}} - 3 + 3\lambda)c^{\infty}_{jm2} + (9 + 4\text{Bo}^{\text{d}} + 6\lambda)c^{\infty}_{jm0}\Big] \tag{57}$$

and for $j > 1$,

$$g^{(0)}_{jm} = \frac{2j+1}{\sqrt{j(j+1)}(1+\lambda-2\text{Bo}^{\text{s}}+j\delta)}\times \Big[3c^{\infty}_{jm2} - 2\sqrt{j(j+1)}c^{\infty}_{jm0}\Big] \tag{58}$$

The migration induced by the conception of surfactant can be obtained by inserting (57) into (24).

Acknowledgements

JTS acknowledges support from a National Research Council – National Institute of Standards and Technology postdoctoral fellowship. PMV acknowledges partial financial support by NSF grant CBET-0846247.

References

1 J. Bławzdziewicz, P. Vlahovska and M. Loewenberg, *Phys. A*, 2000, **276**, 50–80.
2 P. Wohl and S. Rubinow, *J. Fluid Mech.*, 1974, **62**, 185–207.
3 S. P. Sutera and R. Skalak, *Annu. Rev. Fluid Mech.*, 1993, **25**, 1–19.
4 P. C. Chan and L. G. Leal, *J. Fluid Mech.*, 1979, **92**, 131–170.
5 L. G. Leal, *Annu. Rev. Fluid Mech.*, 1980, **12**, 435–476.
6 J. Hanna and P. Vlahovska, *Phys. Fluids*, 2010, **22**, 013102.
7 L. G. Leal, *Advanced transport phenomena*, Cambridge University Press, 2007.
8 H. Goldsmith and S. Mason, *Nature*, 1961, **190**, 1095–1096.
9 W. Hiller and T. Kowalewski, *Exp. Fluids*, 1987, **5**, 43–48.
10 J. D. Martin and S. D. Hudson, *New J. Phys.*, 2009, **11**, 115005.
11 J. T. Cabral and S. D. Hudson, *Lab Chip*, 2006, **6**, 427–436.
12 S. D. Hudson, J. T. Cabral, W. J. Goodrum, K. Beers and E. Amis, *Appl. Phys. Lett.*, 2005, **87**, 081905.
13 S. Anna, N. Bontouz and H. Stone, *Appl. Phys. Lett.*, 2003, **82**, 364–6.
14 S. Anna and H. Mayer, *Phys. Fluids*, 2006, **18**, 121512.
15 D. T. Wasan, J. J. McNamara, S. M. Shah, K. Sampth and N. Aderangi, *J. Rheol.*, 1979, **23**, 181–207.
16 B. Madivala, S. Vandebril, J. Fransear and J. Vermant, *Soft Matter*, 2009, **5**, 1717–1727.
17 Y. Pawar and K. J. Stebe, *Phys. Fluids*, 1996, **8**, 1738–1751.
18 C. D. Eggleton, Y. Pawar and K. J. Stebe, *J. Fluid Mech.*, 1998, **385**, 79–99.
19 D. A. Edwards, H. Brenner and D. T. Wasan, *Interfacial transport processes and rheology*, Butterworth-Heinemann, Boston, 1991.
20 B. Cichocki, B. U. Felderhof and R. Schmitz, *Physicochem. Hyd.*, 1988, **10**, 383–403.
21 B. U. Felderhof, *J. Chem. Phys.*, 2006, **125**, 124904.
22 S. D. Hudson, *Rheol. Acta*, 2010, **49**, 237–243.
23 A. Helmy and D. Barthès-Biesel, *J. Mech. Theor. Appl.*, 1983, **1**, 859–880.
24 G. Danker, P. M. Vlahovska and C. Misbah, *Phys. Rev. Lett.*, 2009, **102**, 148102.
25 A. R. Edmonds, *Angular momentum in quantum mechanics*, Princeton University Press, Princeton, 1960.
26 P. M. Vlahovska, J. Bławzdziewicz and M. Loewenberg, *Phys. Fluids*, 2005, **17**, 103103.
27 P. M. Vlahovska and R. Gracia, *Phys. Rev. E: Stat., Nonlinear, Soft Matter Phys.*, 2007, **75**, 016313.

